ORIGINAL ARTICLE

Nano-biomarker-Based Surface-Enhanced Raman Spectroscopy for Selective Diagnosis of Gallbladder and Liver Injury

Sanghwa Lee[1] · Eunyoung Tak[2] · Yu Jeong Cho[3,4] · Jiye Kim[2] · Jooyoung Lee[2] · Ryunjin Lee[2] · Kwanhee Lee[2] ·
Minsung Kwon[2] · Young-In Yoon[5] · Sung-Gyu Lee[5] · Jung-Man Namgoong[4] · Jun Ki Kim[1,2]

Abstract

During living donor liver transplantation, a number of blood vessels and bile ducts are anastomosed while the liver and gall-bladder are resected in the donor and recipient. Early detection and treatment of complications after surgery by evaluating the function of blood vessels and the biliary tract is crucial. A biosensing chip that can monitor patient health status from the bile excreted during the recovery process has been developed using a surface-enhanced Raman sensing chip. Surface-enhanced Raman spectroscopy signals of bile obtained from normal bile duct ligation and gallbladder damage mouse models using a cautery device were identified and analyzed. The surface-enhanced Raman chip with a nanometer-level porous structure can selectively separate the nanometer biomarkers and measure the Raman signal. Through the detection of nanometer biomarkers in the bile and comparative analysis of histopathology, the Raman signal in the damaged gallbladder was compared with that caused by liver damage due to bile duct ligation, showing that it becomes a biosensing chip for monitoring recovery.

Sanghwa Lee, Eunyoung Tak, and Yu Jeong Cho have contributed equally to this work.

✉ Jung-Man Namgoong
   namgoong2940@gmail.com

✉ Jun Ki Kim
   kim@amc.seoul.kr

[1] Biomedical Engineering Research Center, Asan Medical Center, Seoul 05505, Republic of Korea

[2] Department of Convergence Medicine, Asan Medical Center, University of Ulsan College of Medicine, Seoul 05505, Republic of Korea

[3] Department of Surgery, Hanyang University Guri Hospital, Hanyang University School of Medicine, Guri 11923, South Korea

[4] Department of Surgery, Asan Medical Center, University of Ulsan College of Medicine, Seoul 05505, Republic of Korea

[5] Division of Liver Transplantation and Hepatobiliary Surgery, Department of Surgery, Asan Medical Center, University of Ulsan College of Medicine, Seoul 05505, Republic of Korea

1 Introduction

Living donor liver transplantation involves the surgical resection of diseased or malfunctioning liver and its replacement with a portion of a healthy liver from a living donor. The surgical technique used for recipients involves using a right lobe graft and anastomoses of blood vessels such as the hepatic artery, hepatic vein, portal vein, inferior vena cava, and bile duct [1]. If the patency of these blood vessels is not smooth after surgery, liver function deteriorates [2]. Therefore, to evaluate the proper function of blood vessels and the biliary tract, liver Doppler ultrasonography and vascular reconstruction computerized imaging should be performed at regular intervals to detect and treat complications early [3]. Biliary tract complications, such as bile leakage around the biliary anastomosis or biliary narrowing, are common in liver transplantation [4, 5]. In the case of bile leakage, if the bile is properly drained through the drainage tube placed during surgery, the leakage of bile stops over time with ductal wound healing. Biliary stenosis can cause jaundice, pruritus, or liver failure and should be treated by widening the narrowed stenosis site by inserting a stent into the biliary tract [6]. The drainage of bile is usually performed

by placement of a drainage tube in the biliary tract from the outside of the liver. Since a cauterizer is used to excise the biliary tract and blood vessels during organ transplantation surgery, heat damage can cause inflammation, which may cause further complications [7]. In addition, as liver transplantation requires the long-term administration of immunosuppressants [8], the risk of infection is very high, particularly in the early stages of transplantation [9]. As the presence of a bile drainage tube after surgery exposes the patient to the risk of infection, it is important to track the recovery of the biliary tract so that the drainage tube can be removed as soon as recovery from the biliary injury is confirmed.

To prevent complication-mediated liver malfunction, diagnosis of the biliary injury is usually made from a biopsy of the tissue to determine the pathological inflammation of the existing organs and tissues [10]. However, tissue biopsy is invasive, and biopsied samples do not guarantee representativeness. Though the occurrence of liver and biliary tract-related inflammation can be detected by measuring the levels of inflammatory cytokines, such as interleukin (IL)-2, tumor necrosis factor-α, and IL-18 from the blood [11], it is difficult to identify the inflamed organ. Therefore, it is necessary to find a novel, low-invasive, and precise biomarker that can identify the presence of bile duct injury.

Biomarkers that can be targeted in vivo are cells (~ tens of µm), erythrocytes (~ 8 µm), bacteria (~ 1 µm), viruses (~ 400 nm), exosomes (several nm to tens of nm depending on their size), proteins, or the smaller molecules, such as cell-free nucleic acids, which are likely to be distributed in body fluids, including a small amount in the blood and urine [12–14]. In several cases, various biomarkers are mixed in biological by-products, if nanometer biomarkers can be selectively detected, results with less noise can be obtained, and the accuracy can be improved [15]. Therefore, the development of a device that can rapidly detect these factors is crucial.

There is an increasing demand for high-sensitivity biosensors that can detect nano-molecules rapidly and accurately [16, 17]. A technique that can potentially address this issue is the Raman spectroscopy system [18], involving spectroscopic analysis that measures the inelastic scattering of light particles of a laser that is incident on a biomarker. Organic and inorganic molecules have their own Raman shift spectrum; therefore, the Raman analysis is a useful measurement method for detecting chemical species in samples. Raman spectroscopy technology has the strongest application potential as a fingerprinting technology for diagnosing diseases in complex organisms, such as living organisms, with the advantage of having multiple detection and functionality of more than tens of multiple detections due to the narrow signal bandwidth [19]. Recently, Raman measurement at a single-molecule scale has been reported with the

surface-enhanced Raman method based on the nanostructure [20, 21]. In a previous study, a surface-enhanced Raman chip based on a nanorod array was fabricated, and selectively enhanced Raman signals were obtained by filtering the nano-biomarkers in urine [22, 23]. By utilizing the ZnO nanostructure framework as a method for manufacturing the surface-enhanced Raman spectroscopy (SERS) chip, ZnO nanostructures can be synthesized in a solution method at a relatively low temperature (80–90 °C), taking advantage of the large-scale, low cost, and diversity of substrate selection [24]. In addition, it is possible to control the size of the biomarker to be measured by controlling the porosity according to the growth conditions of the nanostructures [25].

In this study, a change in the Raman signal was measured by simulating the damage caused by the biliary obstruction that occurs during liver transplantation by manufacturing a bile duct ligation (BDL)-type animal model. In addition, the Raman signal of inflammation caused by heat damage during liver transplantation was measured through the cauterization of the gallbladder as shown in Fig. 1. Through these results, we confirmed that a surface-enhanced Raman bio-sensing chip based on nano-biomarker detection that can monitor the patient's condition from bile excreted from liver transplant patients is possible.

2 Materials and Methods

2.1 Bile Duct Ligation

Anesthesia was induced by the inhalation of 4 vol% isoflurane and maintained with 1.5–2.0 vol% isoflurane in 100% oxygen at a flow rate of 1 L/min. The liver was lifted with a moistened (0.9% NaCl solution) cotton swab such that the ventral side of the liver stuck to the diaphragm and the hilum was clearly visible. The bile duct was exposed by the caudal movement of the gut. A 5–0 silk suture was placed around the bile duct and secured with two surgical knots. A second cranial ligation was added in the same manner but did not dissect the bile duct in-between. A 0.9% NaCl solution was applied to the peritoneal cavity, and the abdominal organs were replaced in their physiological positions. The peritoneum and skin were closed with a simple continuous suture with 5–0 silk, and the operation area was sterilized with betadine, followed by 70% ethanol (two to three times) using cotton swabs. Intraperitoneal injection of tramadol 0.25 mg/kg was performed immediately after surgery.

2.2 Thermal Cauterization Treatment

The mice were anesthetized following the same protocol for bile duct ligation described above, and the abdomen was opened. The liver was moved with a wet cotton swab to
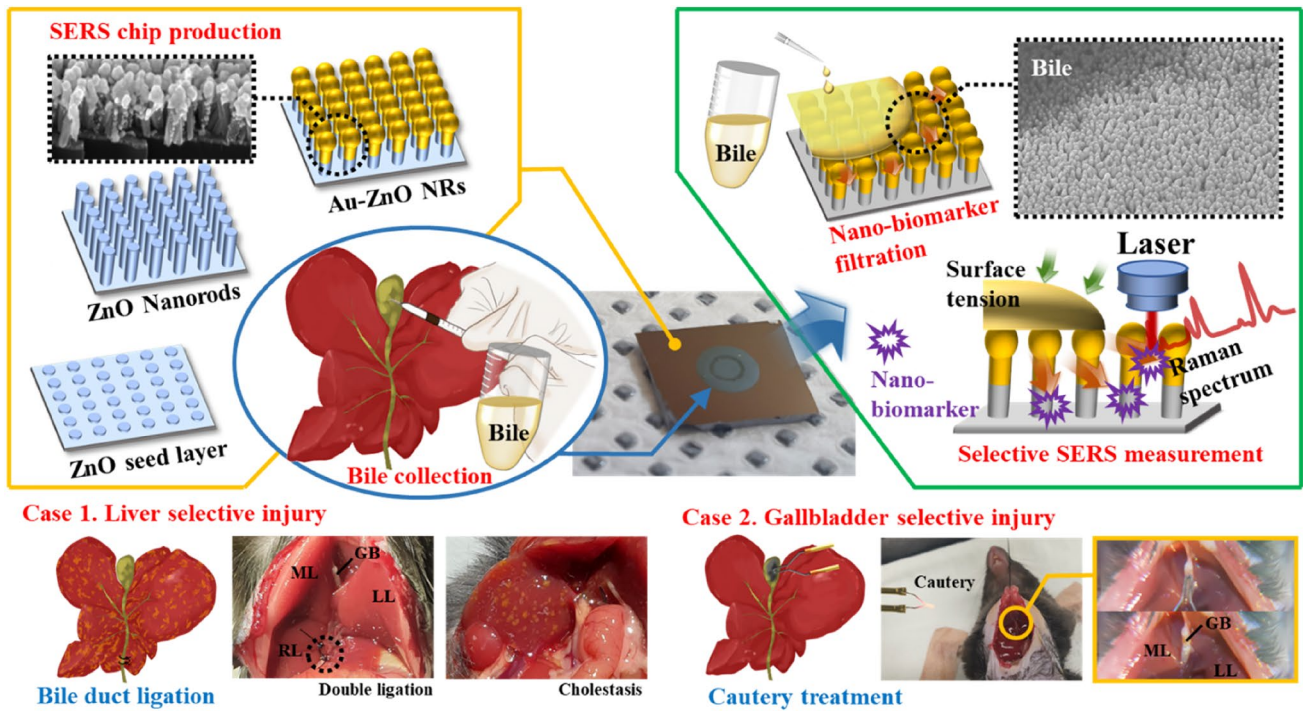
Fig. 1 Outline of animal model development and nanometer biomarker Raman measurement. *GB* Gallbladder, *ML* Median Lobe, *LL* Left Lobe, *RL* Right Lobe

reveal the gallbladder. The gallbladder was cauterized with high-temperature cautery (Change-A-Tip, Bovie, USA).

2.3 Blood Sampling and Laboratory Tests

Whole blood samples were collected from the inferior vena cava of anesthetized mice. The collected blood was allowed to clot for 30 min at 24 °C and centrifuged at $2500 \times g$ for 20 min at 4 °C. To separate the serum from the clotted cells, the transparent upper phase was transferred into new tubes. The serum AST and ALT levels were detected using an automated analyzer (Hitachi 7180, Tokyo, Japan).

2.4 Western Blot

Protein lysates were obtained by homogenized liver tissues in radioimmunoprecipitation assay buffer (Cat#89900, Thermo Fisher Scientific, US). Approximately 15 μg of liver tissue proteins were separated by 15% polyacrylamide gel electrophoresis and transferred to a nitrocellulose membrane for the subsequent steps. The membranes were blocked with 5% bovine serum albumin (Cat#82-100-6, Millipore Corporation, USA) in Tris-buffered saline-Tween-20 and then incubated with primary antibody. The levels of lipocalin-2 (Cat#ab63929, Abcam, UK) and vimentin (Cat#sc-6260, Santa Cruz Biotechnology, USA) were observed. Protein signals were detected by enhanced chemiluminescence

(ECL; Cat#NCI34095, Thermo Fisher Scientific) system and captured using Luminograph II (Cat#WSE-6200, Atto, Japan). For the loading control, the blots were washed and re-probed for actin using horseradish peroxidase, conjugated monoclonal β-actin antibody (A3854; Sigma-Aldrich, USA).

2.5 Histology Analysis

The liver and gallbladder tissues from each group were fixed in 4% paraformaldehyde (pH 7.4; Sigma-Aldrich) and embedded in paraffin blocks. The paraffin blocks were sectioned into 4-μm-thick slides, and the sections were deparaffinized, rehydrated, and stained with hematoxylin and eosin. The morphological changes to the liver tissues were observed using a light microscope (BX53 microscope with DP27 camera; Olympus corporation, Tokyo, Japan). For Sirius Red staining, the deparaffinized slides were incubated in Picro-Sirius Red Solution (Cat#ab150681, Abcam).

2.6 Statistical Analyses

The data were analyzed using GraphPad Prism 5.0 software (GraphPad Software, La Jolla, CA, USA). Hepatic tissue injury scores were described as medians and ranges. All the data were described as mean ± standard deviation for ten samples per condition. Immunoblotting data were obtained from two procedures. Statistical one-way analysis

of variance with Bonferroni's correction was performed. A P value < 0.05 was considered statistically significant.

2.7 Surface-Enhanced Raman Sensing Chip Preparation

For filtering the nanometer markers from bile and amplifying the Raman signal, a vertically aligned gold-ZnO nanorod-based surface-enhanced Raman chip, illustrated in Fig. 1, was fabricated. The ZnO nanostructure support was prepared in a hydrothermal method, and a solution was prepared by dissolving 10 mM zinc nitrate hexahydrate and 0.9 mL ammonium hydroxide zinc nitrate hexahydrate (Sigma Aldrich Co., St. Louis, USA) in deionized water. The ZnO nanorods were grown by dipping a Si wafer (LG SILTRON INC., KOREA) in this solution and maintaining it at 90 °C for 50 min. The grown nanorods were 400–600 nm in length, 50 nm in diameter, and 200 nm in thickness. Au was coated on these ZnO nanostructures using a thermal evaporator (Alpha Plus Co., Korea). A SERS chip was prepared by cutting a specimen of Au-ZnO nanorods on Si to a size of 0.5×0.5 mm.

2.8 Raman Measurements and Principal Component Analysis

The bile obtained from the animal model was placed on the SERS chip as a drop of 0.5 μl; additionally, 30 min later, the sample was loaded into a Raman spectroscopy system (FEX-INV, NOST, Korea) attached to a microscope (IX-73, Olympus, Japan), and the measurement was carried out.

A spectrum was obtained by irradiating a Raman 785 nm wavelength laser to the area where the nano-biomarker diffused from the bile drop into the nanostructure. The Raman spectral spectrum was measured in units of 2.5 cm^{-1} for the 450–2100 cm^{-1} spectral region. Fifth order polynomial fitting was performed as a post-signal process, and it was diagrammed through Origin 2018 software. Data grouping was performed by statistical classification on Raman signals using the PCA method and conducted using the XLSTAT 2019 software.

3 Results and Discussion

3.1 Comparison of the Effects of Bile Duct Ligation and Gallbladder Cauterization on Liver Damage

The BDL animal model is a common method for imitating cholestasis, which represents a reduction or obstruction of bile flow [26]. Cholestasis is a frequent consequence of liver transplantation, and severe cholestasis can be associated with irreversible liver damage requiring re-transplantation

[27]. In the BDL model, the duct that secretes bile from the gallbladder to the duodenum is blocked and the bile refluxes into the liver, resulting in cholestasis (Fig. 1, BDL).

Liver transplantation is commonly accompanied by cholecystectomy (gallbladder ablation). Cholecystectomy is an operative procedure on the biliary tract, first described by Carl Langenbuch in 1882 [28]. During a cholecystectomy, the cystic duct and cystic artery are ligated and incised with electrical surgical cutting by the thermal effect of high-frequency cautery. During this procedure, the gallbladder is removed, and the common bile duct is partly damaged by heat. To mimic these injuries in animal models, a gallbladder thermal cauterization model was developed in this study (Fig. 1, Cautery treatment).

As cholestasis is a well-known cause of liver injury with complex pathological cascades [29], pathological changes in the liver tissue were observed. Histological examination of the liver showed tissue necrosis and lymphatic infiltration in the liver parenchyma in BDL mice (Fig. 2a). In addition, the total bilirubin (TBIL), aspartate aminotransferase (AST), and alanine aminotransferase (ALT), the serum markers related to liver damage, were significantly elevated (Fig. 2b). Lipocalin-2, a protein that reflects apoptosis in liver tissue, and vimentin, which stabilizes type I collagen and causes inflammation-related histological changes in the liver, were also significantly elevated (Fig. 2c). However, with respect to gallbladder cautery, there were no differences in the indicators of liver tissue damage between normal and damaged liver tissue. This finding is based on tests to confirm reproducibility in several animals, and it is completely differentiated within the standard deviation range. In the case of BDL, for all liver function evaluation values including TBIL, AST, and ALT, the error range is sufficient to not overlap, so it is sufficiently effective as a specified model for liver damage to review Raman spectroscopy performance.

3.2 Assessment of Gallbladder Damage Via Histopathology

As the gallbladder is an organ that stores bile, the inside of the gallbladder is tightly surrounded by epithelial cells to protect it from damage caused by the bile acid. The epithelium forms mucosal folds, giving it elasticity. The lamina propria, located close to the epithelium, consists of loose connective tissue, through which veins and arterioles pass and lymphocytes migrate. Below the lamina propria lies the muscularis layer and the adventitia layer [30]. In the normal tissue sample, the epithelium surrounded the inside through the mucosal folds (Fig. 3a). In the BDL tissue sample, most of the epithelium was intact while the mucosal folds were extended. In the gallbladder cauterization tissue sample, the epithelium was partly lost (Fig. 3a). Further investigation of the collagen connective tissue staining with Picro Sirius
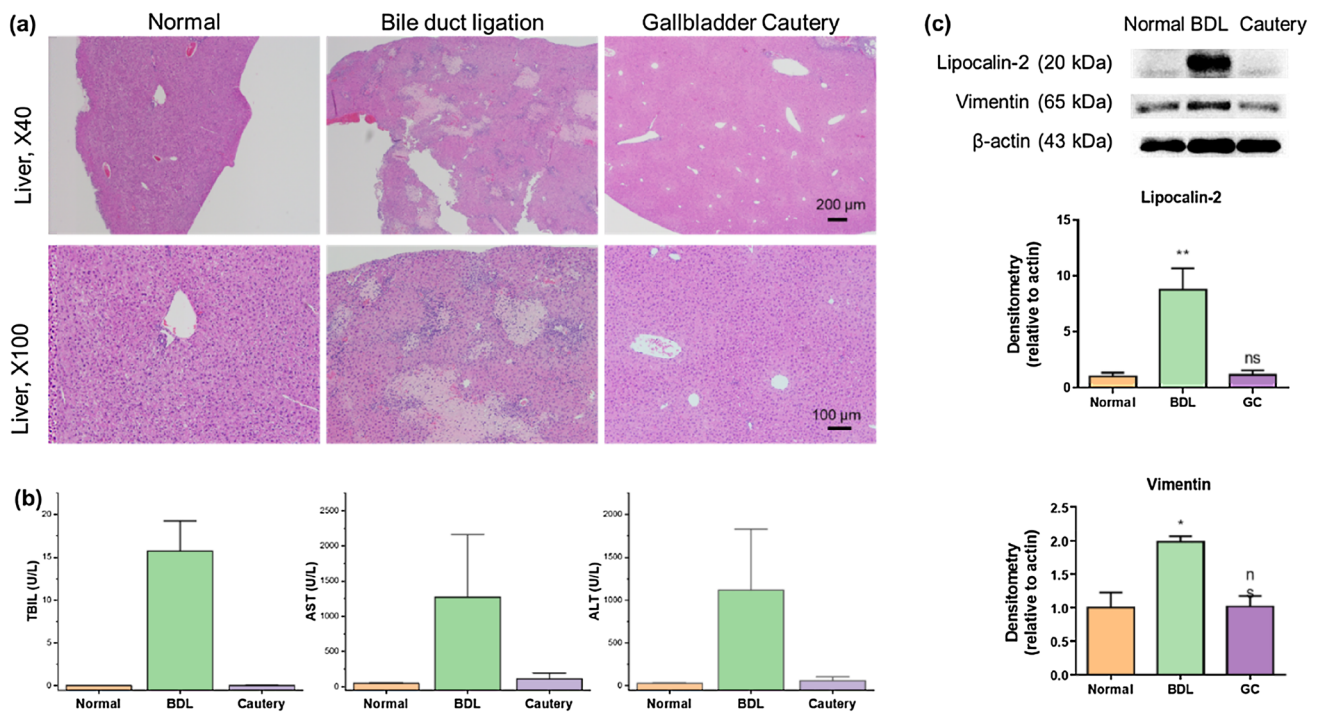
Fig. 2 Evaluation of liver damage and liver function impairment **a** Hematoxylin and Eosin staining result of liver tissues from normal, bile duct ligation (BDL), and gallbladder cautery (Cautery) groups observed under ×40 or ×100 magnification. Scale bar, 200 μm and 100 μm for each magnification. **b** Total bilirubin (TBIL) (U/L), aspartate aminotransferase (AST) (U/L), and alanine aminotrans- ferase (ALT) (U/L) levels were measured in the serum of each group. **c** Liver damage-related protein expression in the normal, BDL, and cautery groups with relative density. All expressions are normalized to β-actin and compared to the Normal group. *$p < 0.05$; **$p < 0.01$; *ns* not significant

Red staining confirmed the epithelium surrounding the collagen connective tissue layer in the normal and BDL groups. However, in the gallbladder cauterization group, the collagen layer was completely exposed to the lumen. Therefore, protection of the gallbladder tissue by epithelial cells after thermal cauterization is difficult.

3.3 Signal Analysis Through Raman Spectra

The area diffused in the spherical direction from the bile dropped on the Au-ZnO-based SERS nanochip for nano-biomarker detection appeared darker than the bare area. This area resulted from the diffusion of the nanometer biomarker into the nano-porous area. Following confirmation that the beam spot was located in this area by opening the laser front-shutter, Raman spectroscopic measurement was performed. The Raman signals of normal, BDL, and gallbladder cauterization were plotted as shown in Fig. 4. The mean spectrum is plotted with solid lines, and the standard deviation is plotted with shades. In the case of normal and BDL, there was no specific peak or appearance of a small peak; however, in the case of gallbladder cauterized bile, remarkable peaks appeared. Main peaks were observed at 881 cm^{-1} for tryptophan [31, 32], 912 cm^{-1} for glucose [32, 33], 1002 cm^{-1} [31,

34], 1033 cm^{-1} [31, 35], 1605 cm^{-1} for phenylalanine [32, 35], 1163 cm^{-1} for tyrosine [31, 32], 1242 cm^{-1} for amide III [32, 36], and 1374 cm^{-1} for nucleic acid [35, 37]. The assignment of each major peak and its reference are shown in Table 1. In particular, the collagen-related assignment was observed at 1002, 1033, 1163, and 1242 cm^{-1}, and the correlation with the gallbladder cautery result is shown in Fig. 3. In hematoxylin and eosin staining, normal and BDL inner epithelial cells remained closed; however, the gallbladder cauterization group was characterized by inner epithelial cells that remained open at the heat injury site a few days after the procedure. In the BDL group, the tensile strain was applied to the gallbladder to the extent that internal wrinkles disappeared; however, the internal epithelial cells remained closed. Considering that more lymphatic cells were observed in the adventitia (or serosa) of the gallbladder of BDL mice than in that of normal mice (Fig. 3a), inflammatory changes in the gallbladder were not reflected in the bile components. This suggests that if the gallbladder epithelium is intact, the inflammatory changes in the gallbladder and liver do not affect the SERS-measurable contents of the bile. Therefore, the presence of internal epithelial cells is a major factor in determining the release of the nanometer markers contributing to Raman signals. This approach was also verified by the
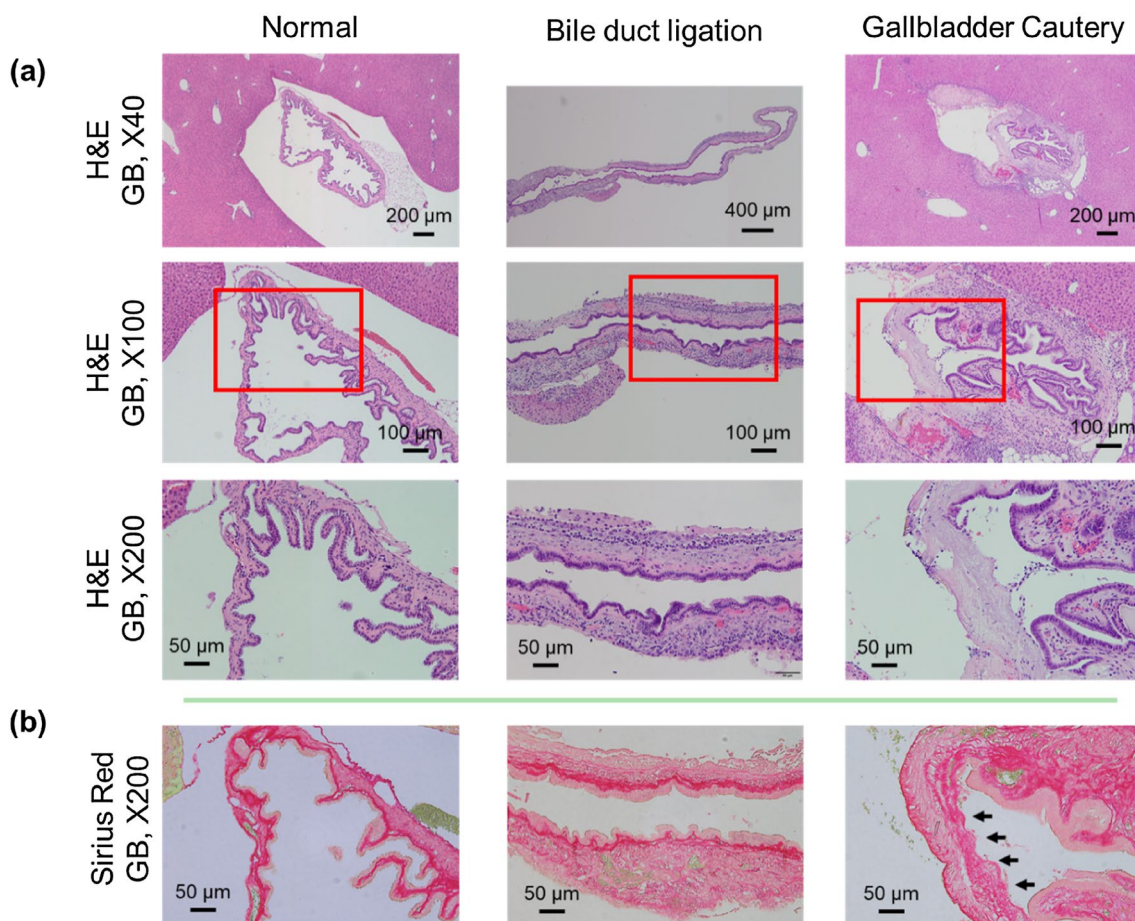
Fig. 3 Gallbladder damage evaluation **a** hematoxylin and eosin (H&E) staining result of the gallbladder and nearby liver tissue in normal, bile duct ligation (BDL), and gallbladder cautery (Cautery) group observed under ×40, ×100, and ×200 magnification with a scale bar. **b** Picro-Sirius Red staining result of the gallbladder in the normal, BDL, and cautery group under ×200 magnification. A serial section of the same sample used for H&E staining was stained and observed. The black arrows indicate the damaged inner epithelium of the gallbladder

Fig. 4 Averaged Raman spectra in the normal (black line), bile duct ligation (blue line), and gallbladder cautery (red line) animal models. The standard deviation in each Raman spectrum is the smeared color, and the value for the main peak is expressed numerically
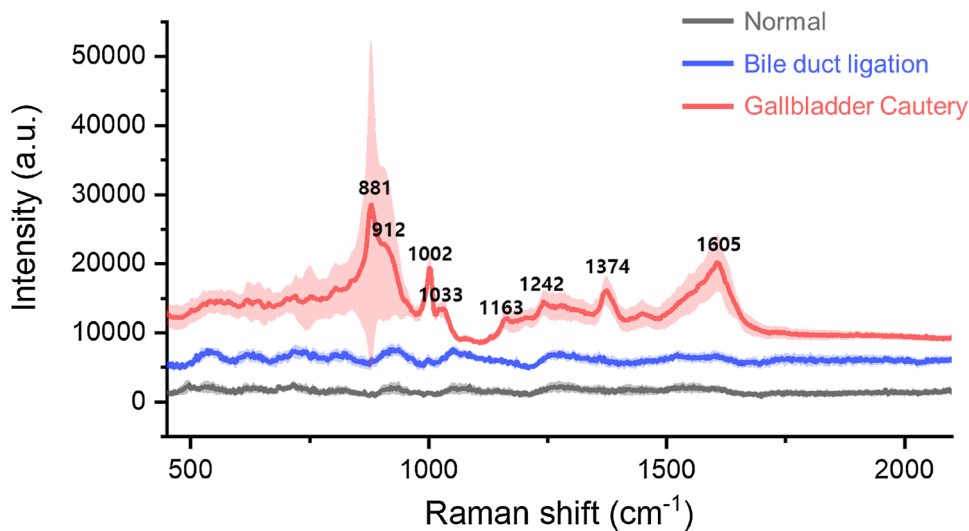
Table 1 Assignment of Raman peak in the gallbladder cautery sample

Peak (cm^{-1})	Assignment	References
881	Tryptophan	[31, 32]
912	Glucose	[32, 33]
1002	Phenylalanine (collagen assignment)	[31, 34]
1033	Phenylalanine (collagen assignment)	[31, 35]
1163	Tyrosine (collagen type I)	[31, 32]
1242	Amide III of collagen	[32, 36]
1374	Nucleic acid	[35, 37]
1605	Phenylalanine, tyrosine	[32, 35]

Sirius Red staining results, and as shown in Fig. 3b, it can be seen that Sirius Red is darkly stained in the area where the collagen is highly distributed. In the normal and BDL groups, high-density collagen is closed by inner epithelial cells; however, in the gallbladder cauterization group, collagen regions are exposed to the lumen of the gallbladder. Therefore, it is postulated that damage to the internal epithelium caused by heat injury can cause the flow of collagen-related biomarkers into the bile. In addition, thermal injury can cause necrosis, which induces rupture of the cell membrane and nucleic envelope with DNA leakage [38]. During necrotic cell death, cell-consisting materials can leak into neighboring body fluids; in cases involving gallbladder injury, the leaked fluid is likely to be bile.

The gallbladder is surrounded by epithelial cells to protect it from damage such as that caused by bile acids. Epithelial cell function was not affected even though the mucosal folds were expanded in BDL. However, damage caused by thermal cauterization was confirmed by Hematoxylin and Eosin and Sirius red staining results. Increased amounts of various biomaterials in the bile, detected through the extraction process, have been found where tissues have been exposed to bile acids due to epithelial cell dysfunction. This increase was revealed by the SERS sensing chip capable of detecting nanometer biomarkers. The collagen leak was confirmed by the Sirius Red staining histopathology results. These findings demonstrate that damage to the inner epithelial cells of the gallbladder can be sensed through the SERS signal of the bile.

3.4 Principal Component Statistical Analysis of Results

The spectrum for the nanometer biomarkers of gallbladder cautery sample consists of multiple variables (peaks) and monitoring through a single variable is required for sensing. Principal component analysis (PCA) is a statistical analysis of functions with an algorithm that reduces the variables [22, 39], and is a useful approach to minimize the variables
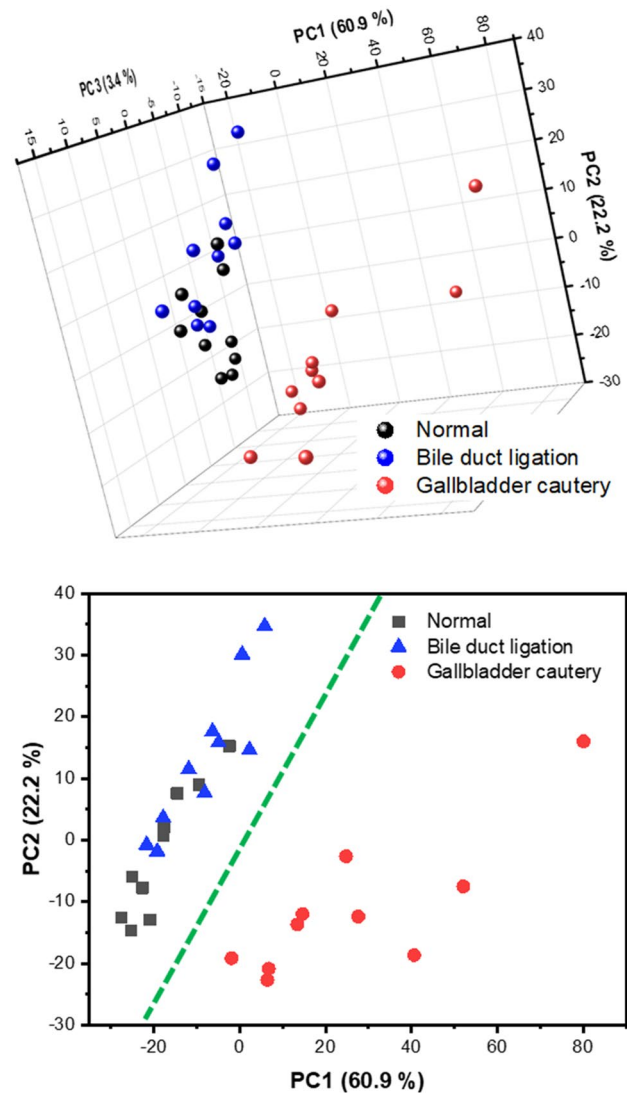

Fig. 5 **a** Analysis results up to the third principal component of normal, bile duct ligation, and gallbladder cautery Raman results; **b** providing a baseline for distinguishing gallbladder cauterization results in the PC1 and PC2 planes (green dashed line)

obtained from this Raman spectrum. The PCA results of Raman spectra for normal, BDL, and gallbladder cautery models are shown in Fig. 5a; additionally, the variability of PC1, PC2, and PC3 were 60.9%, 22.2%, and 3.4%, respectively. As shown in Fig. 5b, the baseline that distinguishes injuries caused by cautery in the PC1 and PC2 planes is well determined. Conversely, there were negligible differences between the normal and BDL models. The results of the Raman signal in the bile indicated that monitoring according to the source of damage occurring during liver transplantation is possible. The Raman signal contains inter-and intra-animal variation. In Fig. 4, except for the 800–950 nm range, the standard deviation was narrow, and the reproducibility was high only for a specific area. Nevertheless, the results

of the thermal cauterization case were sufficiently well differentiated based on the green dotted line in the PCA results of Fig. 5b for the entire Raman signal.

Liver damage due to stenosis of the bile duct means that biomarkers, such as TBIL, AST, and ALT, are monitored using the amount of release into the blood, and damage to the lining of the gallbladder (bile duct) due to thermal cauterization is monitored using nano-biomarkers in the bile. Selective detection of nanometer markers in the bile was confirmed as a Raman signal when internal epithelial cells were destroyed by thermal cauterization. In the thermal cauterization case, tissue staining results revealed that the mucosal layer with high collagen density was exposed to bile, and, as shown in Table 1, the Raman signal was characterized by a substantial contribution from collagen-derived amino acids. Therefore, the contribution of collagen-related amino acids as a candidate for trappable nano-biomarkers in the nano-porous space is large, and monitoring of damage and recovery of epithelial cells inside the gallbladder can be verified by the Raman signal assigned to collagen. Excessive use of electrocautery to control biliary duct bleeding can clinically lead to early postoperative bile leak [31, 32]. Most biliary leaks occur within 1–3 months of liver transplantation and account for 1–25% of biliary complications following transplantation [33, 34]. We suggest that patient morbidity and the hospitalization period may be decreased prompt detection of bile duct damage using Raman spectroscopy. Furthermore, it is anticipated that future research will enable rapid and accessible monitoring of ischemia, which causes damage to the layers of the bile duct, anastomotic stricture due to reperfusion injury, and biloma.

4 Conclusion

To monitor recovery following liver transplantation, a biosensing chip that acquires surface-enhanced Raman signals from the nano-biomarkers in excreted bile was applied. The surface-enhanced Raman chip used in this paper had the advantage of considerably increasing the Raman signal while selectively filtering nanometer markers. An animal model for monitoring the liver and gallbladder (bile duct) injury was developed, and biosensing Raman chip measurement was performed. Liver damage due to bile duct stenosis was induced using BDL in a mouse model, and samples for selective damage to the gallbladder (bile duct) were prepared from gallbladder damage through cauterization. Liver function was evaluated through liver histopathology and blood TBIL, AST, and ALT; liver function was considerably decreased in BDL mice. These results were verified by measuring the lipocalin-2 and vimentin levels in the liver tissue. Hematoxylin and Eosin staining

of the gallbladder confirmed that the epithelium of the gallbladder disappeared only in cases with damage caused by heat cauterization. Moreover, through Sirius Red staining, it was confirmed that collagen was exposed to the inside of the gallbladder due to the disappearance of the epithelium. Raman spectra were obtained for normal, BDL, and cautery samples; additionally, a remarkable peak appeared only in the gallbladder cauterization samples. Most of these peaks are generated by collagen-related sources, including phenylalanine, which is mainly found in bio-samples. Raman signal assignment was consistent with the result of exposure of the high-density collagen region due to epithelium disappearance, as shown in Sirius Red staining. In conclusion, PCA allowed the determination of the criteria for detecting heat injury in the gallbladder.

Declarations

Conflict of interest The authors declare no conflict of interest.

References

1. Seiler, C.A.: The bile duct anastomosis in liver transplantation. Digest Surg. **16**, 102–106 (1999)
2. Yin, C., Zhu, Z.J., Wei, L., Sun, L.Y., Zhang, H.M., et al.: Risk factors for portal vein stenosis in pediatric liver transplantation. Clin. Transplant. **34**, e13992 (2020)
3. Zoepf, T., Maldonado-Lopez, E.J., Hilgard, P., Dechene, A., Malago, M., et al.: Diagnosis of biliary strictures after liver transplantation: Which is the best tool? World J. Gastroenterol. **11**, 2945–2948 (2005)
4. Kochhar, G., Parungao, J.M., Hanouneh, I.A., Parsi, M.A.: Biliary complications following liver transplantation. World J. Gastroenterol. **19**, 2841–2846 (2013)
5. Fang, C., Yan, S., Zheng, S.: Bile leakage after liver transplantation. Open Med. (Wars). **12**, 424–429 (2017)
6. Chang, J.H., Lee, I., Choi, M.G., Han, S.W.: Current diagnosis and treatment of benign biliary strictures after living donor liver transplantation. World J. Gastroenterol. **22**, 1593–1606 (2016)
7. Moy, B.T., Birk, J.W.: A review on the management of biliary complications after orthotopic liver transplantation. J. Clin. Transl. Hepatol. **7**, 61–71 (2019)
8. Best, L.M., Leung, J., Freeman, S.C., Sutton, A.J., Cooper, N.J., et al.: Induction immunosuppression in adults undergoing liver transplantation: a network meta-analysis. Cochrane Database Syst. Rev. **1**, CD013203 (2020)

9. Moini, M., Schilsky, M.L., Tichy, E.M.: Review on immunosuppression in liver transplantation. World J. Hepatol. **7**, 1355–1368 (2015)

10. Kleiner, D.E., Brunt, E.M., Van Natta, M., Behling, C., Contos, M.J., et al.: Design and validation of a histological scoring system for nonalcoholic fatty liver disease. Hepatology **41**, 1313–1321 (2005)

11. Narayanaswamy, B., Gonde, C., Tredger, J.M., Hussain, M., Vergani, D., et al.: Serial circulating markers of inflammation in biliary atresia—evolution of the post-operative inflammatory process. Hepatology **46**, 180–187 (2007)

12. Durand, F., Francoz, C., Asrani, S.K., Khemichian, S., Pham, T.A., et al.: Acute kidney injury after liver transplantation. Transplantation **102**, 1636–1649 (2018)

13. Citores, M.J., Lucena, J.L., de la Fuente, S., Cuervas-Mons, V.: Serum biomarkers and risk of hepatocellular carcinoma recurrence after liver transplantation. World J. Hepatol. **11**, 50–64 (2019)

14. Lewandowska, L., Malyszko, J., Joanna Matuszkiewicz-Rowinska, J.: Urinary and serum biomarkers for prediction of acute kidney injury in patients undergoing liver transplantation. Ann. Transplant. **24**, 291–297 (2019)

15. Panikar, S.S., Banu, N., Haramati, J., Gutierrez-Silerio, G.Y., Bastidas-Ramirez, B.E., et al.: Anti-fouling SERS-based immunosensor for point-of-care detection of the B7–H6 tumor biomarker in cervical cancer patient serum. Anal. Chim. Acta. **1138**, 110–122 (2020)

16. Lee, J.U., Kim, S., Sim, S.J.: SERS-based nanoplasmonic exosome analysis: enabling liquid biopsy for cancer diagnosis and monitoring progression. Biochip J. **14**, 231–241 (2020)

17. Perdomo, S.A., Marmolejo-Tejada, J.M., Jaramillo-Botero, A.: Review-bio-nanosensors: fundamentals and recent applications. J. Electrochem. Soc. **168**, 107506 (2021)

18. Perumal, J., Wang, Y.S., Attia, A.B.E., Dinish, U.S., Olivo, M.: Towards a point-of-care SERS sensor for biomedical and agri-food analysis applications: a review of recent advancements. Nanoscale **13**, 553–580 (2021)

19. Lee, H., Gao, X.H., Kim, Y.P.: Immuno-nanoparticles for multiplex protein imaging in cells and tissues. Biochip J. **12**, 83–92 (2018)

20. Oh, Y.J., Kang, M., Park, M., Jeong, K.H.: Engineering hot spots on plasmonic nanopillar arrays for SERS: a review. Biochip J. **10**, 297–309 (2016)

21. Maccaferri, N., Barbillon, G., Koya, A.N., Lu, G.W., Acuna, G.P., et al.: Recent advances in plasmonic nanocavities for single-molecule spectroscopy. Nanoscale Adv. **3**, 633–642 (2021)

22. Lee, S., Namgoong, J.M., Jue, M., Joung, Y., Ryu, C.M., et al.: Selective detection of nano-sized diagnostic markers using Au-ZnO nanorod-based surface-enhanced raman spectroscopy (SERS) in ureteral obstruction models. Int. J. Nanomed. **15**, 8121–8130 (2020)

23. Lee, S., Namgoong, J.M., Yu, H.Y., Jue, M., Kim, G., et al.: Diagnosis in a preclinical model of bladder pain syndrome using a Au/ZnO nanorod-based SERS substrate. Nanomaterials-Basel. **9**, 224 (2019)

24. Vayssieres, L.: Growth of arrayed nanorods and nanowires of ZnO from aqueous solutions. Adv. Mater. **15**, 464–466 (2003)

25. Jue, M., Lee, S., Paulson, B., Namgoong, J.M., Yu, H.Y., et al.: Optimization of ZnO nanorod-based surface enhanced raman scattering substrates for bio-applications. Nanomaterials-Basel **9**, 447 (2019)

26. Georgiev, P., Jochum, W., Heinrich, S., Jang, J.H., Nocito, A., et al.: Characterization of time-related changes after experimental bile duct ligation. Br. J. Surg. **95**, 646–656 (2008)

27. Ben-Ari, Z., Pappo, O., Mor, E.: Intrahepatic cholestasis after liver transplantation. Liver Transplant. **9**, 1005–1018 (2003)

28. Chauvin, K.L., Oleary, J.P.: Langenbuch, Carl and the first cholecystectomy. Am. Surgeon. **61**, 746–747 (1995)

29. Tag, C.G., Sauer-Lehnen, S., Weiskirchen, S., Borkham-Kamphorst, E., Tolba, R.H., et al.: Bile duct ligation in mice: induction of inflammatory liver injury and fibrosis by obstructive cholestasis. Jove-J. Vis. Exp. (2015). https://doi.org/10.3791/52438

30. Housset, C., Chretien, Y., Debray, D., Chignard, N.: Functions of the gallbladder. Compr. Physiol. **6**, 1549–1577 (2016)

31. Cheng, W.T., Liu, M.T., Liu, H.N., Lin, S.Y.: Micro-Raman spectroscopy used to identify and grade human skin pilomatrixoma. Microsc. Res. Techniq. **68**, 75–79 (2005)

32. Movasaghi, Z., Rehman, S., Rehman, I.U.: Raman spectroscopy of biological tissues. Appl. Spectrosc. Rev. **42**, 493–541 (2007)

33. Krafft, C., Neudert, L., Simat, T., Salzer, R.: Near infrared Raman spectra of human brain lipids. Spectrochim. Acta A Mol. Biomol. Spectrosc. **61**, 1529–1535 (2005)

34. Frank, C.J., Mccreery, R.L., Redd, D.C.B.: Raman-spectroscopy of normal and diseased human breast tissues. Anal. Chem. **67**, 777–783 (1995)

35. Chan, J.W., Taylor, D.S., Zwerdling, T., Lane, S.M., Ihara, K., et al.: Micro-Raman spectroscopy detects individual neoplastic and normal hematopoietic cells. Biophys. J. **90**, 648–656 (2006)

36. Pezzotti, G., Boffelli, M., Miyamori, D., Uemura, T., Marunaka, Y., et al.: Raman spectroscopy of human skin: looking for a quantitative algorithm to reliably estimate human age. J. Biomed. Opt. **20**, 065008 (2015)

37. Dovbeshko, G.I., Gridina, N.Y., Kruglova, E.B., Pashchuk, O.P.: FTIR spectroscopy studies of nucleic acid damage. Talanta **53**, 233–246 (2000)

38. Zong, W.X., Thompson, C.B.: Necrotic death as a cell fate. Gene Dev. **20**, 1–15 (2006)

39. Yao, F.Z., Coquery, J., Le Cao, K.A.: Independent Principal Component Analysis for biologically meaningful dimension reduction of large biological data sets. BMC Bioinformatics (2012). https://doi.org/10.1186/1471-2105-13-24